

## COMMUNICATION

# The NMR and X-ray Structures of the *Saccharomyces cerevisiae* Vts1 SAM Domain Define a Surface for the Recognition of RNA Hairpins

Tzvi Aviv<sup>1,2</sup>, Andrew N. Amborski<sup>3</sup>, X. Sharon Zhao<sup>3</sup>, Jamie J. Kwan<sup>4</sup>  
Philip E. Johnson<sup>3</sup>, Frank Sicheri<sup>1,2\*</sup> and Logan W. Donaldson<sup>4\*</sup>

<sup>1</sup>Program in Molecular Biology and Cancer, Samuel Lunenfeld Research Institute, Mount Sinai Hospital, 600 University Ave. Toronto, Ont., Canada M5G 1X5

<sup>2</sup>Department of Molecular and Medical Genetics, University of Toronto, Toronto, Ont., Canada M5S 1A8

<sup>3</sup>Department of Chemistry, York University, 4700 Keele St. Toronto, Ont., Canada M3J 1P3

<sup>4</sup>Department of Biology, York University, 4700 Keele St. Toronto, Ont., Canada M3J 1P3

The SAM domain of the *Saccharomyces cerevisiae* post-transcriptional regulator Vts1 has a high affinity towards RNA hairpins containing a CUGGC pentaloop. We present the 1.6 Å X-ray crystal structure of the Vts1 SAM domain in its unliganded state, and the NMR solution structure of this domain in its RNA-bound state. Both structures reveal a canonical five helix SAM domain flanked by additional secondary structural elements at the N and C termini. The two structures are essentially identical, implying that no major structural rearrangements occur upon RNA binding. Amide chemical shift changes map the RNA-binding site to a shallow, basic patch at the junction of helix  $\alpha 5$  and the loop connecting helices  $\alpha 1$  and  $\alpha 2$ .

© 2005 Elsevier Ltd. All rights reserved.

\*Corresponding authors

**Keywords:** sterile alpha motif; NMR spectroscopy; X-ray crystallography; translational repression

The sterile alpha motif (SAM) domain is a relatively small, yet functionally versatile ligand-binding domain with a documented affinity for other SAM domains, lipids and RNA.<sup>1,2</sup> The first RNA-binding SAM domain was identified in Smaug, a translational repressor involved in the early development of *Drosophila*.<sup>3–5</sup> In the 3' untranslated region (UTR) of *nanos* mRNA, its natural substrate, Smaug binds a hairpin motif containing a 5'-CUGGC-3' pentaloop termed SRE (Smaug recognition element). The crystal structure of the minimal SRE-binding fragment of Smaug in its RNA-free form revealed a SAM domain fused to a pseudo HEAT repeat analogous topology domain as one integral unit.<sup>6</sup> Structure-directed mutagenesis studies demonstrated that a basic patch located exclusively on the SAM domain is sufficient for all aspects of high-affinity SRE RNA recognition.<sup>7,8</sup>

The SAM domain of *Saccharomyces cerevisiae* Vts1, the object of this study, binds RNA *in vitro* with the same sequence specificity and affinity as Smaug.<sup>7</sup> Vts1 promotes the degradation of a reporter gene containing three consecutive SRE sequences. However, unlike Smaug, which acts upon *nanos* gene transcripts, no endogenous targets of Vts1 have been identified. Though precise functional roles for Vts1 remain undefined, Vts1 has been implicated in the general processes of vesicular transport<sup>9</sup> and sporulation.<sup>10</sup> The Smaug and Vts1 SAM domains bind RNA hairpins bearing either a 5'-CUGGC-3' pentaloop or a 5'-CUGG-3' tetraloop with great affinity.<sup>7</sup> Substitutions of Cyt1, Gua3 and Gua4 (bases are numbered according to their position in the pentaloop) with any other base reduces binding by more than two orders of magnitude, while substitutions of Ura2 or Cyt5 have no effect.<sup>7</sup>

Towards understanding the structural aspects of RNA recognition by Vts1, the crystal structure of its unliganded SAM domain and the NMR structure of the SAM domain in its RNA-bound state were determined. Amide chemical shift differences

Abbreviations used: SAM, sterile alpha motif; SRE, Smaug recognition element.

E-mail addresses of the corresponding authors: [sicheri@mshri.on.ca](mailto:sicheri@mshri.on.ca); [logand@yorku.ca](mailto:logand@yorku.ca)

between the free and bound states identify a basic patch that corroborates previous mutagenesis studies. Superposition of the free and bound protein structures indicates that SRE binding does not induce global or local conformational changes in the Vts1 SAM domain.<sup>10</sup>

### Delineating the boundaries of the Vts1 SAM domain

Initially, we expressed a large fragment of Vts1 (residues 407–523) that encompassed the canonical SAM domain (residues 448–512) and a sizable N-terminal region fused to glutathione-S-transferase. Although Vts1 does not possess a C-terminal pseudo HEAT repeat analogous topology domain like its counterpart Smaug, deletion analysis indicated that sequences flanking the canonical SAM domain sequence were important for protein folding and solubility. The core RNA-

binding fragment of Vts1 was further delimited by treatment with the protease thermolysin. The boundaries of a protease-resistant fragment (residues 436–523) were deduced by matrix-assisted laser desorption/ionization time-of-flight mass spectrometry and tandem mass spectrometry sequencing of trypsinized peptides. The thermolysin-resistant fragment was functionally indistinguishable from the larger Vts1<sup>407–523</sup> fragment on the basis of SRE RNA binding affinity ( $K_d \approx 30$  nM) and specificity (Figure 1(a)).

### The crystal structure of the unliganded Vts1 SAM domain

Crystals of the thermolysin-resistant fragment of Vts1 were obtained using a commercially available sparse matrix screen. Phase determination was performed by single isomorphous replacement with anomalous scattering on a mercury derivative of an

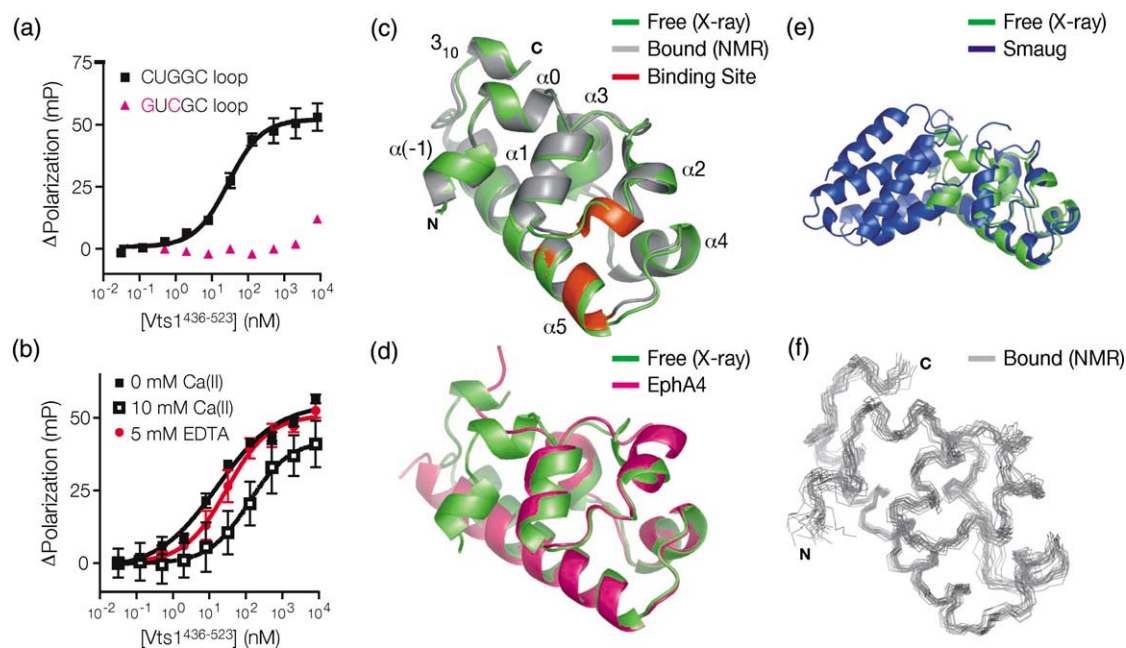


**Figure 1.** The crystal structure of free Vts1 SAM and the NMR structure of SRE-bound Vts1 SAM are essentially identical. A gene fragment encompassing the SAM domain (residues 407–523) of *S. cerevisiae* VTS1 was amplified by PCR methods and inserted into a modified pGEX vector. The resulting glutathione-S-transferase fusion protein was purified by affinity chromatography from soluble extracts of *E. coli* BL21(DE3) grown in a BioFlow 110 fermentor at 25 °C. Isotopically labeled Vts1<sup>407–526</sup> was obtained from fermentations in minimal M9 medium containing 1.0 g/l [U-98%] [<sup>15</sup>N]ammonium chloride and 4.0 g/l [U-99%] [<sup>13</sup>C]glucose as the sole sources of nitrogen and carbon, respectively. Vts1<sup>407–523</sup> was cleaved from the fusion protein with TEV protease. Proteins were further purified and buffer-exchanged using S-100 gel-filtration chromatography. For crystallography, the 13 kDa Vts1 fragment was digested with thermolysin to produce a minimal 10 kDa fragment, Vts1<sup>436–523</sup>, that was purified further by heparin chromatography. A 19 nt SRE RNA (5′-GGAGGCUCUGGCAGCUUUC-3′) was prepared in milligram quantities for NMR spectroscopy by phage T7 RNA polymerase-driven, *in vitro* transcription.<sup>17</sup> The SRE RNA was purified by denaturing 20% PAGE and electroeluted. Renaturation of the SRE RNA hairpin was achieved by rapidly chilling a solution that was preheated to 94 °C. (a) A fluorescence polarization binding assay<sup>7</sup> of the thermolysin-resistant Vts1 SAM domain demonstrates high-affinity binding for the SRE (5′-AGGCUCUGGCAGUCU-3′) but not a mutant SRE bearing substitutions at the first and third loop positions. (b) A modest decrease in binding affinity is observed when either 5 mM EDTA or 10 mM Ca<sup>2+</sup> is present in the binding buffer. (c) Superposition of the free Vts1 SAM domain crystal structure with the bound NMR structure reveals no significant conformational changes. The SRE binding site is indicated in red. Superposition of the crystal structures of the Vts1 SAM domain with the (d) EphA4 SAM domain and the (e) Smaug SAM domain. (f) Superposition of the 20 lowest energy NMR structures of the RNA-bound Vts1 SAM domain.

Ala472Cys mutant. A single copy of Vts1<sup>436–523</sup> and an anomalous scattering ion (possibly Ca<sup>2+</sup>) is present in the asymmetric unit. Though a divalent metal ion (Mg<sup>2+</sup>, Ca<sup>2+</sup>, Sr<sup>2+</sup>, or Ba<sup>2+</sup>) is required for crystallization, fluorescence polarization binding assays performed in the presence of calcium and chelating agents revealed that metal ions do not play a significant role in SRE binding (Figure 1(b)). The crystal structure at 1.6 Å resolution (Figure 1(c); Table 1) comprises residues 442–523 of Vts1, with six disordered N-terminal residues (436–441). The hallmark five-helix bundle ( $\alpha$ 1– $\alpha$ 5, residues 455–515) of the SAM domain is apparent and superimposes well with the crystal structure of the EphA4 SAM domain (RMSD 1.3 Å; Figure 1(d))<sup>11</sup> and, to a lesser

degree, with the Smaug SAM domain (RMSD 2.2 Å; Figure 1(e)). Two short  $\alpha$ -helices denoted  $\alpha$ 0, (residues 449–453) and  $\alpha(-1)$ , (residues 443–447) and one  $3_{10}$  helix (residues 520–522) pack against the N terminus of helix  $\alpha$ 1 and the C-terminal portion of helix  $\alpha$ 5. In Smaug, these additional structural elements are donated by the pseudo HEAT repeat analogous topology domain.<sup>8</sup> From sequence comparisons, helix  $\alpha$ 0 is conserved among all fungal homologs of Vts1, while helix  $\alpha(-1)$  and the  $3_{10}$  helix are conserved only among a sub-group of closely related yeast species.

**Table 1.** Data collection, phasing and refinement statistics of the free Vts1 SAM domain crystal structure

	Vts1	A472C-HgCl
<i>Data collection</i>		
Space group	<i>P</i> 2 <sub>1</sub> 2 <sub>1</sub> 2 <sub>1</sub>	<i>P</i> 2 <sub>1</sub> 2 <sub>1</sub> 2 <sub>1</sub>
Cell dimensions		
<i>a</i> , <i>b</i> , <i>c</i> (Å)	27.31, 27.60, 99.87	27.38 27.89, 99.91
$\alpha$ , $\beta$ , $\gamma$ (deg.)	90, 90, 90	90, 90, 90
Resolution (Å)	26.6–1.60	26.86–1.80
	(1.66–1.6)	(1.86–1.8)
<i>R</i> <sub>sym</sub> or <i>R</i> <sub>merge</sub>	0.038 (0.184)	0.067 (0.183)
<i>I</i> / $\sigma$ <i>I</i>	26.7 (5.3)	11.1 (4.0)
Completeness (%)	92.4 (95.9)	93.5 (99.9)
Redundancy	5.1 (4.0)	3.3 (3.4)
<i>Refinement</i>		
Resolution (Å)	49.8–1.6	
No. reflections	9250	
<i>R</i> <sub>work</sub> / <i>R</i> <sub>free</sub>	0.205/0.255	
No. atoms		
Protein	681	
Calcium	1	
Water	75	
<i>B</i> -factors		
Protein (Å <sup>2</sup> )	14.9	
Water (Å <sup>2</sup> )	24.4	
RMS deviations		
Bond lengths (Å)	0.01	
Bond angles (deg.)	1.33	

A stock solution of Vts1 was prepared in 20 mM Hepes (pH 7.0), 100 mM NaCl. Crystals were grown from microseeded drops of 3 mM Vts1 mixed in equal parts with a reservoir solution containing 50 mM Tris-HCl (pH 8.5), 30% (w/v) PEG 4000, 200 mM NH<sub>4</sub>Cl, 10 mM CaCl<sub>2</sub>. In 24–48 h, crystals of 0.1 mm × 0.03 mm × 0.03 mm appeared and were diffracted on a Rigaku compact laboratory instrument and processed using Crystal Clear software (Rigaku). The diffraction data were obtained from one crystal. To obtain experimental phases, crystals of an Ala472Cys mutant were soaked for 3 h in reservoir solution substituted with 40% PEG 4000 and saturated with HgCl<sub>2</sub>. Phases were calculated from single isomorphous replacement with anomalous scattering and were used to calculate experimental electron density maps with SHARP.<sup>19</sup> An homology model of Vts1 SAM was fit manually into the electron density map, followed by iterative rounds of manual and automatic adjustments against the native dataset using the CCP4 package.<sup>20</sup> The crystal packing of Vts1 SAM is unusually tight with a Matthews coefficient of 1.9 Å<sup>3</sup>/Da and 34.1% (v/v) solvent content. The highest resolution shell is shown in parentheses. Ramachandran statistics calculated using PROCHECK<sup>21</sup> indicate 91.5% residues in the most favored regions and 8.5% in additionally allowed regions.

**Table 2.** Statistics for the ensemble of NMR structures of the RNA-bound Vts1 SAM domain

Experimental observations	
Distance constraints	
Total NOE	1778
Intraresidue	757
Interresidue	1021
Sequential ( $ i-j =1$ )	442
Medium-range ( $1 <  i-j  < 5$ )	321
Long-range ( $ i-j  > 5$ )	258
Hydrogen bonds	34
Dihedral angle restraints	
$\phi/\psi$	73
Violations	
Mean number of NOE violations > 0.5 Å	0
Mean number of NOE violations > 0.3 Å	1.3
Number of dihedral angle violations > 5°	0
Deviations from idealized geometry	
Bond lengths (Å)	0.009 ± 0.000
Bond angles (deg.)	1.166 ± 0.046
Impropers (deg.)	1.265 ± 0.071
RMSD from the average structure (Å)	
Backbone $\alpha$ 1– $\alpha$ 5 (455–515)	0.66 ± 0.14
Heavy $\alpha$ 1– $\alpha$ 5 (455–515)	1.38 ± 0.17
Backbone (444–522)	0.77 ± 0.14
Heavy (444–522)	1.49 ± 0.16

Samples of Vts1<sup>407–523</sup> for NMR spectroscopy varied from 0.7–1.2 mM in 20 mM sodium phosphate (pH 7.4), 150 mM NaCl, 0.02% (w/v) NaN<sub>3</sub>, and 10% <sup>2</sup>H<sub>2</sub>O. Spectra were acquired at 20 °C on a Bruker Avance 600 MHz spectrometer and a Varian Inova 800 MHz spectrometer (NANUC, Edmonton, AB). A Vts1-RNA complex was prepared by titrating protein into an RNA solution and following changes in RNA imino resonances at 5 °C. Backbone assignments of free and bound Vts1 were obtained from HNCACB, CBCA(CO)NH and HNCO spectra. Very few resonances in an unstructured N-terminal region extending from positions 407–442 that would have otherwise made interpretation of the spectra difficult. Side-chain assignments of bound Vts1 were obtained from (H)C(CO)NH, H(C)(CO)NH, and HCCH-TOCSY spectra. NOE crosspeaks from <sup>15</sup>N-HSQC-NOESY and <sup>13</sup>C-HSQC-NOESY spectra (100 ms mixing time) were calibrated from 1.8–5.0 Å using the CALIBA module of CYANA v2.0. All spectra were processed with NMRPipe<sup>22</sup> and interpreted with NMRView.<sup>23</sup> Dihedral ( $\phi/\psi$ ) angle restraints were derived from backbone chemical shifts using TALOS.<sup>24</sup> Initial structures were calculated with CYANA 2.0.<sup>25</sup> Hydrogen bond restraints (O–HN, 1.8–2.1 Å; O–N, 2.7–3.0 Å) were determined by assessing the initial ensemble for backbone O–HN distances < 2.4 Å and a bond angles < 25°. Of the 200 structures calculated with XPLOR-NIH 2.9.9,<sup>26</sup> the best 100 structures according to lowest energy were subjected to one round of water refinement.<sup>27</sup> Analysis of the 20 best water-refined structures using PROCHECK-NMR<sup>28</sup> indicates that 92.5% of the amino acid residues are located in the most favored region of the Ramachandran map, with 7.3% in additionally allowed regions and 0.1% in generously allowed regions.

## The NMR structure of the Vts1 SAM domain in the RNA-bound state

Many RNA-binding domains place a secondary structure element into the RNA major groove or present a cleft for RNA docking.<sup>12,13</sup> These structural features are absent from the unliganded Vts1 SAM domain, as revealed by X-ray crystallography. To determine if RNA-binding induces structural changes in the Vts1 SAM domain which, in turn, create a deep binding pocket or protrusion, we determined the solution structure of Vts1<sup>407–523</sup> bound to 19 nt SRE RNA pentaloop hairpin at a stoichiometric ratio of 1:1. The overall backbone RMSD of the 20 lowest energy conformers is 0.77 Å based on 1729 NOE-derived distance restraints and 73 database-derived torsion angle restraints (Figure 1(f); Table 2). The resulting structure of the Vts1 SAM domain in its bound state is essentially identical with the X-ray structure of the Vts1 SAM domain in its free state. The backbone (N, C<sup>α</sup>, C') atoms of the free X-ray structure and the bound NMR structure of Vts1 SAM domains superimpose with an RMSD of 1.26 Å, comparable to the precision of the NMR structure determination (Figure 1(c)). This high degree of structural similarity leads us to conclude

that SRE binding does not induce a major conformational rearrangement of the Vts1 SAM domain.

## Mapping the SRE RNA-binding site

RNA binding induces a number of <sup>1</sup>H, <sup>15</sup>N chemical shift changes in the Vts1 SAM domain (Figure 2(a)). The majority of these changes localize to a conserved positively charged surface patch defined by the α1-α2 loop and the N terminus of helix α5 (Figure 2(b)). Of the six amide resonances (Leu465, His466, Leu496, Gly497, Ala498, and Lys501) that shift significantly upon RNA binding, all but Leu496 are absolutely conserved among Vts1 homologs, including *Drosophila* Smaug.<sup>7,8</sup> Significant chemical shift changes were observed also for the guanidino N<sup>ε</sup>/H<sup>ε</sup> resonances of Arg464 and Arg500 (data not shown), suggesting that these charged groups contact RNA. Among Vts1 homologs, Arg464 is absolutely conserved, while Arg500 may be substituted with other polar amino acid residues. Overall, the binding site deduced by chemical shift mapping corroborates previous mutagenesis studies on Vts1<sup>7</sup> and Smaug.<sup>7,8</sup>

Among 11 C<sup>α</sup> atoms in the deduced RNA binding site (residues 464–467, 496–502), the free and bound states superimpose to 0.62 Å RMSD (Figure 1(c)).

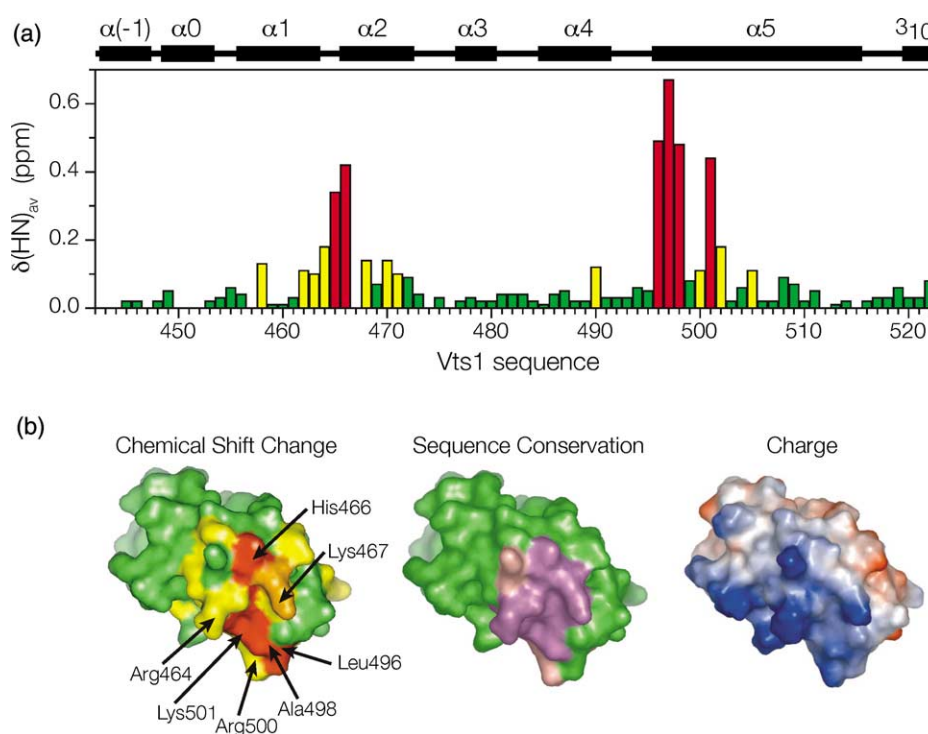


**Figure 2.** The RNA-binding surface on the Vts1 SAM domain. (a) Weighted-averaged<sup>18</sup> amide <sup>1</sup>H and <sup>15</sup>N chemical shift changes upon SRE RNA binding where  $\delta_{av}(\text{HN}) = [\delta\text{H}^2 + (\delta\text{N}/5)^2]/2^{1/2}$ . Bars are colored according to the magnitude of the chemical shift change (red, >0.3 ppm; yellow, >0.1 ppm). (b) Chemical shift changes, sequence conservation, and electrostatic charge are mapped onto the surface of the free X-ray structure of Vts1 SAM domain. HSQC perturbations are colored according to (a). The linewidth of Lys467 sharpens significantly upon RNA binding and is colored orange. Sequence identity (in purple) and sequence similarity (in pink) among Vts1 homologs coincides with the SRE binding surface deduced from chemical shift perturbations. The RNA-binding site demonstrates basic charge distribution (red; negative potential; blue, positive potential). Molecular structure representations and electrostatic calculations were made with pyMOL (<http://pymol.sourceforge.net>).

This indicates that the RNA-binding site on the SAM domain exists in a preconfigured, competent state for SRE binding. Moreover, the shallow depth and limited size of the binding site suggests that the SAM domain may discriminate only a portion of the SRE.

SAM domain-mediated protein-protein interactions typically occur through two surfaces termed mid-loop (ML) and end-helix (EH), as observed in the structures of the Tel SAM domain homo-oligomer,<sup>14</sup> the Yan/Mae SAM domain heterodimer,<sup>15</sup> and the Ph/Scm SAM domain heterodimer.<sup>16</sup> The RNA-binding surface does not overlap the corresponding ML surface and partially overlap the corresponding EH surfaces of the Vts1 SAM domain. If Vts1 SAM engages other proteins through its EH or ML surfaces, these protein-protein interactions may regulate Vts1 function either by obscuring SRE binding or by recruiting additional factors necessary for transcript regulation.

### Protein Data Bank accession codes

Coordinates of Vts1 SAM in its unbound and SRE-bound forms have been deposited in the Protein Data Bank with accession identifiers 2D3D and 2B6G, respectively.

### Acknowledgements

The authors thank P. S. Metalnikov and P. O'Donnell for assistance with mass spectrometry. This research was funded by the Canadian Institutes for Health Research (to P.J., F.S., and L.D), and the National Cancer Institute of Canada (to F.S.).

### References

- Kim, C. A. & Bowie, J. U. (2003). SAM domains: uniform structure, diversity of function. *Trends Biochem. Sci.* **28**, 625–628.
- Ponting, C. P. (1995). SAM: a novel motif in yeast sterile and *Drosophila* polyhomeotic proteins. *Protein Sci.* **4**, 1928–1930.
- Smibert, C. A., Lie, Y. S., Shillinglaw, W., Henzel, W. J. & Macdonald, P. M. (1999). Smaug, a novel and conserved protein, contributes to repression of nanos mRNA translation *in vitro*. *RNA*, **5**, 1535–1547.
- Dahanukar, A., Walker, J. A. & Wharton, R. P. (1999). Smaug, a novel RNA-binding protein that operates a translational switch in *Drosophila*. *Mol. Cell*, **4**, 209–218.
- Smibert, C. A., Wilson, J. E., Kerr, K. & Macdonald, P. M. (1996). Smaug protein represses translation of unlocalized nanos mRNA in the *Drosophila* embryo. *Genes Dev.* **10**, 2600–2609.
- Green, J. B., Edwards, T. A., Trincao, J., Escalante, C. R., Wharton, R. P. & Aggarwal, A. K. (2002). Crystallization and characterization of Smaug: a novel RNA-binding motif. *Biochem. Biophys. Res. Commun.* **297**, 1085–1088.
- Aviv, T., Lin, Z., Lau, S., Rendl, L. M., Sicheri, F. & Smibert, C. A. (2003). The RNA-binding SAM domain of Smaug defines a new family of post-transcriptional regulators. *Nature Struct. Biol.* **10**, 614–621.
- Green, J. B., Gardner, C. D., Wharton, R. P. & Aggarwal, A. K. (2003). RNA recognition *via* the SAM domain of Smaug. *Mol. Cell*, **11**, 1537–1548.
- Dilcher, M., Kohler, B. & von Mollard, G. F. (2001). Genetic interactions with the yeast Q-SNARE VTI1 reveal novel functions for the R-SNARE YKT6. *J. Biol. Chem.* **276**, 34537–34544.
- Deutschbauer, A. M., Williams, R. M., Chu, A. M. & Davis, R. W. (2002). Parallel phenotypic analysis of sporulation and postgermination growth in *Saccharomyces cerevisiae*. *Proc. Natl Acad. Sci. USA*, **99**, 15530–15535.
- Stapleton, D., Balan, I., Pawson, T. & Sicheri, F. (1999). The crystal structure of an Eph receptor SAM domain reveals a mechanism for modular dimerization. *Nature Struct. Biol.* **6**, 44–49.
- Draper, D. E. (1999). Themes in RNA-protein recognition. *J. Mol. Biol.* **293**, 255–270.
- Messias, A. C. & Sattler, M. (2004). Structural basis of single-stranded RNA recognition. *Accs Chem. Res.* **37**, 279–287.
- Tran, H. H., Kim, C. A., Faham, S., Siddall, M. C. & Bowie, J. U. (2002). Native interface of the SAM domain polymer of TEL. *BMC Struct. Biol.* **2**, 5.
- Qiao, F., Song, H., Kim, C. A., Sawaya, M. R., Hunter, J. B., Gingery, M. *et al.* (2004). Derepression by depolymerization; structural insights into the regulation of Yan by Mae. *Cell*, **118**, 163–173.
- Kim, C. A., Sawaya, M. R., Cascio, D., Kim, W. & Bowie, J. U. (2005). Structural organization of a Sex-comb-on-midleg/polyhomeotic copolymer. *J. Biol. Chem.* **280**, 27769–27775.
- Milligan, J. F., Groebe, D. R., Witherell, G. W. & Uhlenbeck, O. C. (1987). Oligoribonucleotide synthesis using T7 RNA polymerase and synthetic DNA templates. *Nucl. Acids Res.* **15**, 8783–8798.
- Farmer, B. T., II, Constantine, K. L., Goldfarb, V., Friedrichs, M. S., Wittekind, M. & Yanchunas, J., Jr (1996). Localizing the NADP<sup>+</sup> binding site on the MurB enzyme by NMR. *Nature Struct. Biol.* **3**, 995–997.
- de la Fortelle, E. & Bricogne, G. (1997). Maximum-likelihood heavy-atom parameter refinement for multiple isomorphous replacement and multiwavelength anomalous diffraction methods. *Methods Enzymol.* **276**, 472–494.
- Collaborative Computational Project No. 4 (1994). The CCP4 suite: programs for protein crystallography. *Acta Crystallog. sect. D*, **50**, 760–763.
- Laskowski, R. A., MacArthur, M. W., Moss, D. S. & Thornton, J. M. (1993). PROCHECK: a program to check the stereochemical quality of protein structures. *Proteins: Struct. Funct. Genet.* **12**, 345–364.
- Delaglio, F., Grzesiek, S., Vuister, G. W., Zhu, G., Pfeifer, J. & Bax, A. (1995). NMRPipe: a multidimensional spectral processing system based on UNIX pipes. *J. Biomol. NMR*, **6**, 277–293.
- Johnson, B. A. & Blevins, R. A. (1994). NMRVIEW: a computer program for the visualization and analysis of NMR data. *J. Biomol. NMR*, **4**, 603–614.
- Cornilescu, G., Delaglio, F. & Bax, A. (1999). Protein backbone angle restraints from searching a database for chemical shift and sequence homology. *J. Biomol. NMR*, **13**, 289–302.

25. Guntert, P., Mumenthaler, C. & Wuthrich, K. (1997). Torsion angle dynamics for NMR structure calculation with the new program DYANA. *J. Mol. Biol.* **273**, 283–298.
26. Schweiters, C. D., Kuzewski, J. J., Tjandra, N. & Clore, G. M. (2003). The XPLOR-NIH molecular structure determination package. *J. Magn. Reson.* **160**, 66–74.
27. Linge, J. P., Williams, R. M., Spronk, C. A., Bonvin, A. M. & Nilges, M. (2003). Refinement of protein structures in explicit solvent. *Proteins: Struct. Funct. Genet.* **50**, 496–506.
28. Laskowski, R., Rullman, J., MacArthur, M., Kaptein, R. & Thornton, J. (1996). ROCHECK-NMR: programs for checking the quality of protein structures solved by NMR. *J. Biomol. NMR*, **8**, 477–486.

*Edited by J. Doudna*

(Received 19 August 2005; received in revised form 23 October 2005; accepted 21 November 2005)  
Available online 7 December 2005